

Complex Plasma Research under Microgravity Conditions: PK-3 Plus Laboratory on the International Space Station

A. G. Khrapak^{1*}, V. I. Molotkov¹, A. M. Lipaev¹, D. I. Zhukhovitskii¹, V. N. Naumkin¹, V. E. Fortov¹, O. F. Petrov¹, H. M. Thomas², S. A. Khrapak^{1,2}, P. Huber², A. Ivlev³, and G. Morfill³

¹ Joint Institute for High Temperature RAS, 125412 Moscow

² Forschungsgruppe Komplexe Plasmen, DLR, Oberpfaffenhofen, Germany

³ Max-Planck-Institute for Extraterrestrial Physics, D-85748, Garching, Germany

Received 29 October 2015, revised 03 December 2015, accepted 09 December 2015

Published online 24 February 2016

Key words Complex plasma, microgravity, phase transition, Mach cone, electrorheological effect.

Complex (dusty) plasmas are composed of weakly ionised gas and charged microparticles and represent the plasma state of soft matter. Due to the "heavy" component — the microparticles — and the low density of the surrounding medium, the rarefied gas and plasma, it is necessary to perform experiments under microgravity conditions to cover a broad range of experimental parameters which are not available on ground. The investigations have been performed onboard the International Space Station (ISS) with the help of the "Plasma Crystal-3 Plus" (PK-3 Plus) laboratory. It was perfectly suited for the formation of large stable liquid and crystalline systems and provided interesting insights into processes like crystallisation and melting, laning in binary mixtures, electrorheological effects due to ac electric fields and projectile interaction with a strongly coupled complex plasma cloud.

© 2016 WILEY-VCH Verlag GmbH & Co. KGaA, Weinheim

1 Introduction

Complex plasmas are plasmas containing small solid particles, typically in the micrometer range, the so-called microparticles. These are dusty plasmas which are specially prepared to study fundamental processes in the strong coupling regime on the most fundamental (kinetic) level, through the observation of individual microparticles and their interactions. Many interesting phenomena can be studied starting from small two-dimensional (2D) and three-dimensional (3D) clusters [1], to larger 2D and 3D systems where collective effects play a dominant role [2].

In laboratory conditions, the microparticles are heavily affected by the force of gravity. Gravity leads to the sedimentation of the particles and can be balanced either by a strong electric field in the sheath of a discharge or through thermophoretic force due to a constant temperature gradient over the microparticle cloud. Additionally, there exist weaker forces like the neutral and ion drag forces, which nevertheless can play a very important role in the total force balance.

Under microgravity conditions, e.g. on the International Space Station (ISS), gravity is negligible. Therefore, the particles are pushed out of the strong electric field region close to the electrodes due to their negative charge and can form large, more or less, homogenous particle clouds in the bulk of the discharge. Under these conditions, weaker forces like the ion drag force and the interparticle interactions become important and often dominate the motion and structure formation in complex plasma.

Since 2001 complex plasma research under microgravity conditions is continuously performed in a Russian-German cooperation onboard the ISS with the long-term laboratories PKE-Nefedov and PK-3 Plus, operational from 2001 to 2005 and from 2006 to 2013, respectively. The first laboratory, PKE-Nefedov, has already provided great insight into the behavior of complex plasma under microgravity conditions [3–6]. Fundamental investigations, like the formation of a particle free void in the center of the microparticle cloud induced by the ion drag

* Corresponding author. E-mail: khrapak@mail.ru

force underestimated by the state of the art theory, which has been improved by the adaption to the new experimental results [7], or the first observation of bcc structures in plasma crystals [3] are only a few of the interesting results obtained there. The follow-up laboratory, PK-3 Plus, has been improved considerably compared to the first one and has been equipped with new diagnostic tools [8]. It has provided the next important step in research of complex plasmas under microgravity conditions. The obtained results are unique and opened up a new interdisciplinary research directions, in particular, related to the field of soft condensed matter. The purpose of this paper is to summarize some of the most important results obtained using the PK-3 Plus laboratory onboard ISS.

2 Short description of PK-3 Plus laboratory

The PK-3 Plus laboratory was developed taking into account the experience obtained during the operation of its precursor PKE-Nefedov.

The PK-3 Plus setup has a well-balanced symmetrically driven rf-electrode system which provides a homogeneous distribution of the plasma with identical sheaths near both electrodes. This is necessary for a homogeneous distribution of the microparticles under microgravity conditions. A cross-sectional and perspective schematic of the microgravity setup, the PK-3 Plus chamber, is shown in Fig. 1 [8]. The vacuum chamber consists of a glass cuvette of form of a cuboid with a quadratic cross section. Top and bottom flanges are metal plates. They include the rf-electrodes, electrical feedthroughs and the vacuum connections. The electrodes are circular plates made from Aluminum with a diameter of 6 cm. The distance between the electrodes is 3 cm. The electrodes are surrounded by a 1.5 cm wide ground shield including three microparticle dispensers on each side. The dispensers are magnetically driven pistons with a storage volume at their ends. The storage volumes are filled with microparticles and covered with a sieve with an adapted mesh size. The microparticles are dispersed through the sieve into the plasma chamber by electromagnetically driven strokes of the piston.

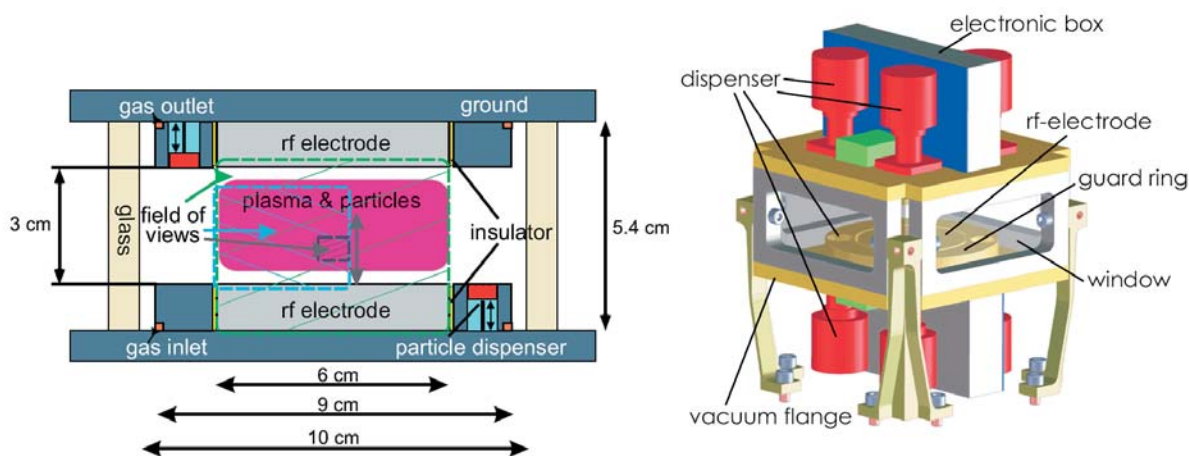


Fig. 1 The sketches show the 2D (left) and 3D (right) view of the PK-3 Plus plasma chamber.

The optical particle detection system consists of laser diodes with cylindrical optics to produce a laser sheet perpendicular to the electrode surface. Three progressive scan CCD-cameras observe the reflected light at 90 degrees with three different magnifications and fields of view. An overview camera has a field of view of $58.6 \times 43.1 \text{ mm}^2$. It shows the full field between the electrodes. A second camera has a field of view of $35.7 \times 26.0 \text{ mm}^2$. It shows the left part of the interelectrode system about half of the full system. A third camera with the highest resolution can be moved along the central axis and has a field of view of $8.1 \times 5.9 \text{ mm}^2$. The latter is used for high precision position measurements of the microparticles. The cameras and lasers are mounted on a horizontal translation stage allowing a depth scan through and, therefore, a 3D view of the complex plasma.

3 Fluid–solid phase transitions in large 3D complex plasmas

We performed experimental investigations of the fluid–solid phase transitions in large 3D complex plasmas under microgravity conditions. These phase changes were driven by manipulating the neutral gas pressure. Detailed analysis of complex plasma structural properties allowed us to quantify the extent of ordering and accurately determine the phase state of the system. Evaluation of various freezing and melting indicators gave further confidence regarding the phase states. It was observed that the system of charged particles can exhibit melting upon increasing the gas pressure, in contrast to the situation in ground-based experiments where plasma crystals normally melt upon reducing the pressure [9]. This illustrates important differences between generic (e.g. similar to conventional substances) and plasma-specific mechanisms of phase transitions in complex plasmas.

The experiments have been carried out in argon at a low rf-power [10]. We used two different sorts of particles in the two distinct experimental runs: SiO₂ spheres with a diameter 1.55 μm and Melamine-Formaldehyde spheres with a diameter 2.55 μm . The experimental procedure, identical in these two runs, was as follows: When the particles formed a stable cloud in the bulk plasma, the solenoid valve to the vacuum pump was opened, which resulted in a slow decrease of the gas pressure p . Then, the valve was closed and the pressure slowly increased due to the gas streaming in. During the pressure manipulation $\simeq 6$ minutes in total, the structure of the particle cloud was observed. The observations covered the pressure range from $p \simeq 15$ Pa, down to the lowest pressure of $p \simeq 11$ Pa and then up to $p \simeq 21$ Pa (see Fig. 2(b)).

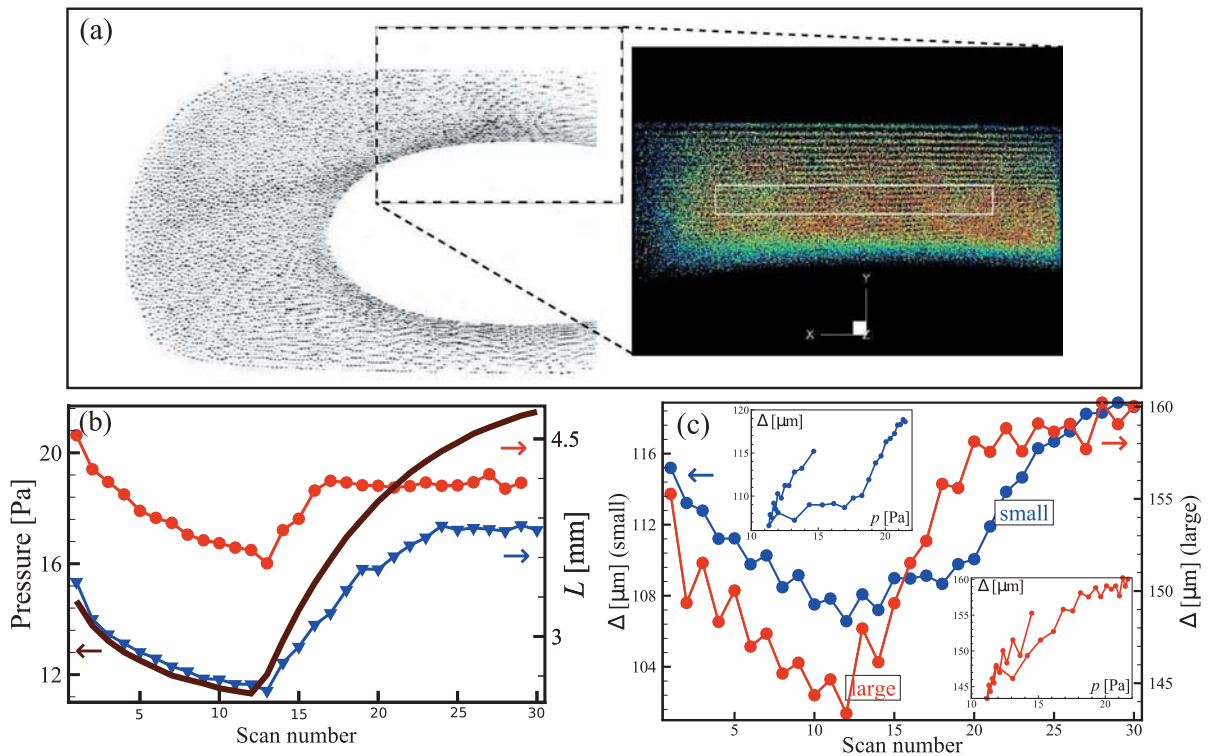


Fig. 2 (a) Side view of the particle cloud (inverted colors) taken with the overview camera (left) and the corresponding field of view of the high resolution camera (right) [particles are color-coded to see solid-like (red) and liquid-like (blue) domains]. Rectangle marks the part of the cloud used for the detailed structural analysis (rectangular box $7.0 \times 0.7 \times 4.5 \text{ mm}^3$). (b) Thickness of the particle cloud in the vertical direction vs. the scan number. Blue triangles (red circles) connected by lines correspond to the system of small (large) particles. The corresponding values of pressure are shown by a brown solid curve (the dependence of pressure on the scan number is almost identical in the two runs). (c) Mean interparticle separation Δ (in the part of the cloud chosen for the analysis) vs. the scan number in the two experimental runs. Blue (red) color corresponds to the system of small (large) particles. Insets show the dependence $\Delta(p)$ demonstrating some hysteresis, which is more pronounced in the system of small particles.

In order to get three-dimensional particle coordinates, 30 scans were performed. Scanning was implemented by simultaneously moving laser and cameras in the direction perpendicular to the field of view with the velocity 0.6 mm/s. Each scan takes $\simeq 8$ s, resulting in the scanning depth of $\simeq 4.8$ mm; the interval between consecutive scans is $\simeq 4$ s. The particle positions were then identified by tomographic reconstruction of the 3D-pictures taken with the high resolution camera observing a region 8×6 mm², slightly above the discharge center.

Let us first discuss the global reaction of the particle cloud on the pressure manipulation. An example of the particle cloud as seen by the overview and high resolution cameras is shown in Fig. 2(a). Figure 2(b) shows the cloud thickness in the vertical direction as a function of the scan number (time) for both the systems of small and large particles. It is observed that the position of the upper boundary is strongly correlated with pressure: It moves downwards (upwards) with the decrease (increase) of p . This has a clear physical explanation. Particles cannot penetrate in the region of strong electric field (sheath) established near the upper electrode. The position of the upper cloud boundary is thus set by the sheath edge. The sheath thickness is roughly proportional to the electron Debye radius λ_{De} which exhibits the following approximate scaling $\lambda_{De} \propto n_e^{-1/2} \propto p^{-1/2}$, where n_e is the electron density. This implies that upon a decrease in the pressure, the particles are pushed farther from the electrode and vice versa, in full agreement with the observations. Thus, the particle component becomes compressed by reducing the pressure and expands when the pressure is increased. The resulting dependence of the mean interparticle distance (in the part of the particle cloud subject to detailed analysis) on the scan number/pressure is shown in Fig. 2(c). The mean interparticle distance Δ is clearly correlated with pressure.

To characterize a structural state of the dusty plasma systems observed we shall use as an example the Raveche-Mountain-Streett criterion of freezing [11], which is based on the properties of the radial distribution function $g(r)$ in the fluid phase. It states that near freezing, the ratio of the values of $g(r)$ corresponding to its first nonzero minimum and to the first maximum, $R = g(r_{min})/g(r_{max})$, is approximately constant, $R \simeq 0.2$. This criterion describes fairly well freezing of the classical Lennard-Jones fluid, but is not truly universal (i.e., the ratio R can somewhat vary for different systems). Figure 3 shows the calculated values of the freezing indicator R for different scans. Applying the threshold condition $R \simeq 0.2$ would imply that the system of small particles melts upon an increase in the neutral gas pressure (second half of the observation sequence), while the system of large particles remains in the solid state. This is consistent with the results of more detailed structural analysis [12].

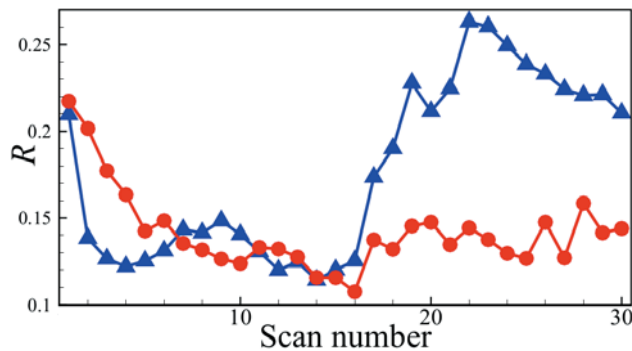


Fig. 3 Freezing indicator R (the Raveche-Mountain-Streett ratio) for complex plasmas composed of small (blue triangles) and large (red circles) particles.

Concerning the structural properties of the observed clouds of particles it should be noted that they are not very homogeneous. For example, typical interparticle separations in peripheral regions close to the cloud boundaries can exceed those in the central part of the cloud by a factor of about 2. For this reason, a relatively small central part of the cloud sketched in Fig. 2(a) has been chosen for the detailed analysis of the structural properties. This part is sufficiently small (especially its vertical extent) so that the system inside is reasonably homogeneous. At the same time, it contains enough particles ($\simeq 10^4$) to yield reasonable statistics. To determine the local structural properties of the three-dimensional particle system we used the bond order parameter method [13, 14], which has been widely used to characterize order in simple fluids, solids, glasses, colloidal suspensions [15], and, more recently, 3D complex plasmas [16]. We were specifically interested in identifying the face-centered cubic (fcc), hexagonal close-packed (hcp), icosahedral (ico), and body-centered cubic (bcc) lattice types. Clear crystalline structures which are dominated by the hcp and fcc lattices were observed. Subsequent increase in the pressure suppressed the particle ordering.

We observed that the solid phase is mostly composed of hcp- and fcc-like particles with only a small portion of bcc-like clusters. A decrease in pressure enhances ordering of the particles. Maximum number of particles in the crystalline state clearly corresponds to the pressure range near the minimum.

4 Phase transition due to the particle charge reduction

We performed experiments to demonstrate a change of the structural properties of the dusty plasma system due to a change of the particle charge. There have been used two-species complex plasmas with one species composed of small ($1.55 \mu\text{m}$) and the other composed of big ($14.9 \mu\text{m}$) particles. The experiments have been carried out in argon gas at a pressure of 10 Pa. The particles are SiO_2 spheres with a diameter $1.55 \mu\text{m}$, the big particles are Melamine-Formaldehyde spheres. The particles of different size do not mix. The smaller particles form an inner cloud close to the discharge centre (with the central area free of particles, see Fig. 4). The big particles form an outer cloud surrounding and confining the smaller one, as it is seen in Fig. 4. The bigger particles can be added to the system. This effectively increases the strength of the confinement and compresses the small particle system.

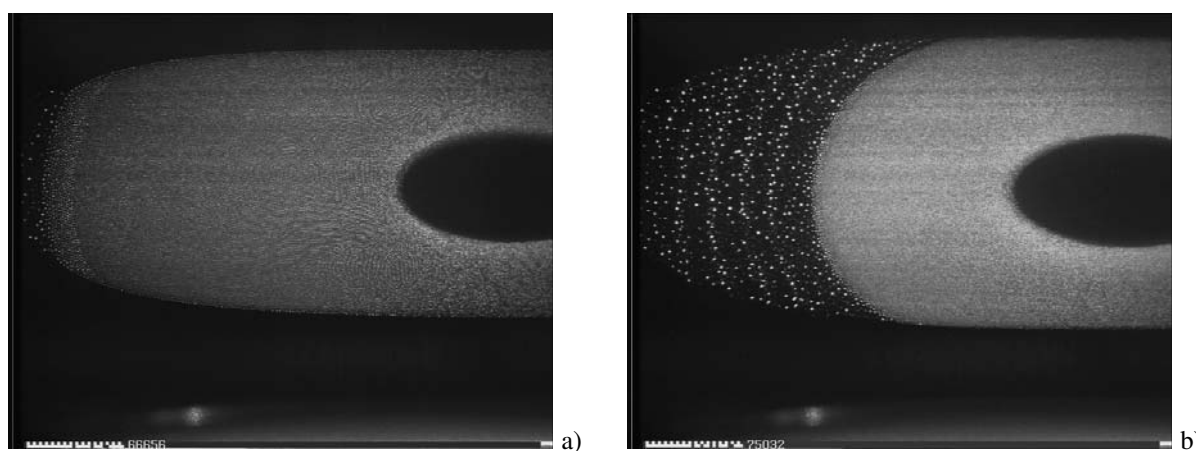


Fig. 4 Video images of dusty plasma system: a) initial system; b) compressed system. Snapshots are obtained by quadrant camera.

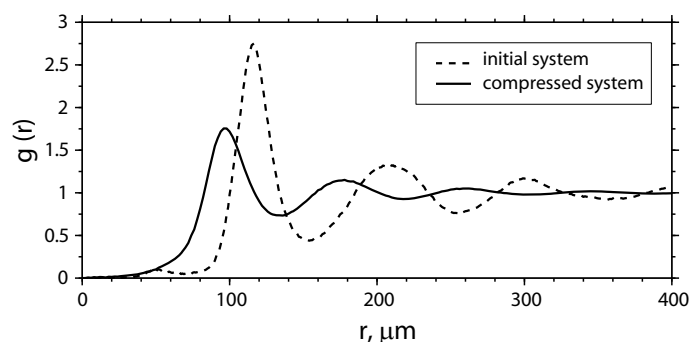


Fig. 5 Change of pair correlation function due to compression by bigger particles.

Fig. 5 demonstrates a change of the pair correlation function for the initial dusty plasma system (only small particles are present) and for the compressed system (with an addition of bigger particles that increases a confinement of the small particles system). Table 1 presents the results of the calculation of some parameters of the dusty subsystem: interparticle distance Δ obtained from the pair correlation function, dust particle density n_p obtained from the processing of the video images received by the high resolution camera, particle charge Q calculated using the orbital motion limited approximation for the experimental plasma parameters. It is seen from Table 1 that the ratio of the first nonzero minimum of $g(r)$ to the first maximum changes from the small value (0.04) pointing to the high ordering in the subsystem (plasma crystal) to the high value (0.21) pointing to melting

of the plasma crystal. Thus, it is a demonstration of the phase transition due to a drop of the absolute magnitude of the particle charge when their density increases.

Table 1 Parameters of the dusty subsystem

$d_p[\mu\text{m}]$	$\Delta[\mu\text{m}]$	$n_p[10^5 \text{ cm}^{-3}]$	$Q[e]$	$\frac{g_{min.}}{g_{max}}$
2.55	125	5.10	2000	0.04
1.55	90	12.0	807	0.21

5 Non-equilibrium phase transition (laning)

A remarkable example of a non-equilibrium phase transition is the formation of "lanes" — a phenomenon occurring in nature when two species of particles are driven against each other. When the driving forces are strong enough, like-driven particles form "stream lines" and move collectively in lanes. Typically, the lanes exhibit a considerable anisotropic structural order accompanied by an enhancement of their (unidirectional) mobility. The phenomenon is most commonly known from pedestrian dynamics in highly populated pedestrian zones [17], but also occurs in different systems of driven particles, such as colloidal dispersions [18, 19], lattice gases [20] and molecular ions [21]. In other words, this is a generic process of considerable interest in different branches of physics.

To study the formation of lanes in complex plasma, experiments with an interpenetration of two clouds of different grain sizes have been performed. In these experiments the structure consisting of particles with 14.9, 9.19, or 6.8 μm in diameter was produced initially. Then, smaller particles with the diameter of 3.4 μm were injected from the left side. The position of the 3.4 μm grain injector is such that these particles are injected in the plane illuminated by the laser sheet. The smaller particles penetrated through the stable structure of bigger particles towards the chamber center. Lane formation was observed in the outer region where the speed of the penetrating grains was high [22]. Figure 6(a) illustrates the formation of lanes. The picture is a superposition of consecutive images: the small penetrating particles can be identified as long tracks, the big particles look like points. It is clearly seen that the penetration of 3.4 μm particles appears in lanes and big particles are arranged into lanes as well. Closer to the middle of the structure the grains speed was reduced and they formed a droplet (see the next section for details).

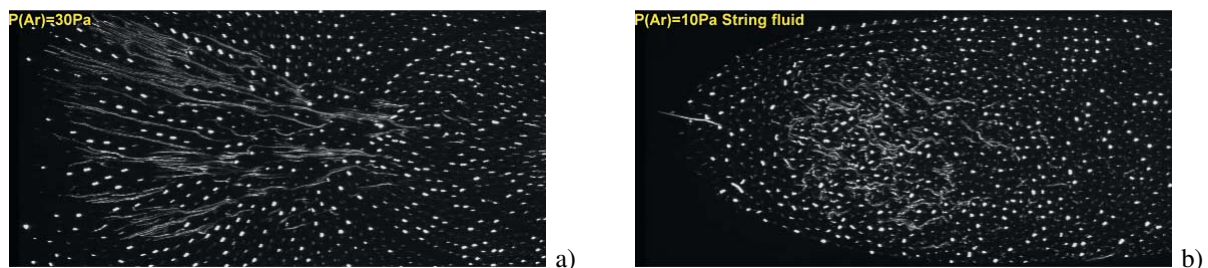


Fig. 6 Penetration of 3.4 μm grains through the structure of 9 μm grains in Ar plasma: a) at pressure 30 Pa, lane formation is seen; b) at pressure 10 Pa, under the action of the low frequency field, no lane formation is seen. Snapshots are obtained by the quadrant camera.

In the case of complex plasma experiments, it is possible to resolve single particle motion and investigate the dynamical regime of laning. We performed experiments in which the big particle cloud was in a string fluid state under the influence of the low frequency electric field (see Section 6 below). This is demonstrated in Fig. 6(b), which has also been obtained as a superposition of consecutive images. It should be noted that lane formation was not observed under these conditions. We suppose that the reason of such behavior is related to the much stronger interaction between big particles, but this requires additional studies [23].

6 Discovery of the electrorheological effect in complex plasmas

As has been known from the beginning of microgravity investigations, the void – the microparticle free region in the center of the discharge – prevents the formation of a homogeneous and isotropic complex plasma clouds. The origin of the void is the ion drag force which often overcomes the electric force in some vicinity of the discharge center and therefore pushes the particles out of the central region. Under certain conditions, the void can be closed. This is very important for many dedicated experiments. With the PK-3 Plus setup three ways of void closure have been detected: by adjusting lowest rf-power (like in the PKE-Nefedov laboratory [4]), by using a symmetrical gas flow, and by low frequency electric excitation [8]. The latter can be used additionally to initiate a phase transition from an isotropic fluid into a so-called electrorheological string fluid.

The formation of such string fluids, or general electrorheological plasmas, is possible due to the manipulation of the interaction potential between the microparticles along the field line. It can be changed from an isotropic screened Coulomb to an asymmetric attractive potential through accelerating ions by an additional ac voltages applied to the electrodes at frequencies above the dust plasma frequency. The ions then produce wake regions above and below the particles along the electric field axis, while the particles cannot respond. It has been shown [24] that the effective interparticle interaction in this case is determined by the time-averaged wake potential. The field-induced interactions in dusty plasmas are identical to interactions in conventional electrorheological fluids with dipoles $d = 0.65Q\lambda v_{ion}/v_{th}$, where Q is the particle charge, λ is the ion screening length, v_{ion} is the ion drift velocity and v_{th} is the ion thermal velocity.

In experiments, the ac voltage at a frequency of 100 Hz was applied to the rf electrodes with the amplitude voltage between 26.6 and 65.6 V varied in steps of 2.2 V. At weak voltages charged particles formed a strongly coupled isotropic fluid phase. As the voltage was increased above a certain threshold, particles rearranged themselves and became more and more ordered, until eventually well-defined particle strings were formed along the direction of the field. In these experiments we used microparticles of different diameters (1.55, 6.8 and 14.9 μm) and Ar gas at pressures between 8 and 15 Pa. The example of the transition to the electrorheological plasma state is presented in Fig. 7. The transition between the isotropic fluid phase and the electrorheological state was fully reversible – decreasing the field brought the particles back into their initial isotropic state. The trend to form strings increased with a particle size, in agreement with theoretical estimates. The molecular dynamic simulations performed with similar parameters yielded remarkable agreement with the experiments.

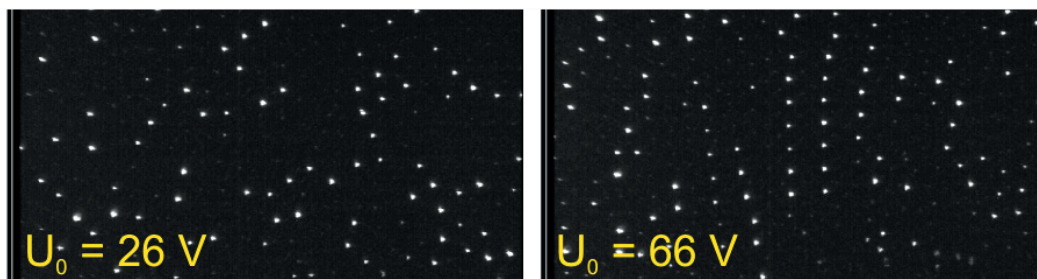


Fig. 7 The transition from an isotropic fluid (left) to a string fluid (right) observed in the PK-3 Plus laboratory onboard the ISS. Particles of 6.8 μm , argon pressure is 10 Pa, interparticle distance is 370 μm . Strings are apart from each other at 580 μm . Snapshots are obtained by the high-resolution camera.

7 Mach cones in 3D complex plasma

The existence of Mach cones in complex plasmas was first predicted in theory by Havnes et al. [25, 26] and later observed in a 2D plasma crystal by Samsonov et al. [27, 28] and Melzer et al. [29]. Mach cones were excited by the electrostatic force from a charged particle moving spontaneously beneath a 2D lattice in refs. [27, 28], and by the radiation force from a spot of focused laser beam scanned across the 2D complex plasma [29]. In these experiments, the observed Mach cones were composed of compressional waves. Shortly afterwards, shear-wave Mach cones composed of single cone, were observed in experiments by Nosenko et al. [30, 31] by using a laser

beam. Inspired by the studies above, various theoretical models [32–37] have been proposed to interpret the observations.

The experimental observations of Mach cones in 3D complex plasmas have been made with the help of the PK-3 Plus laboratory [39–41]. The excitation of the 3D Mach cone was produced by a supersonic projectile moving in a strongly coupled cloud of charged particles. The dust cloud was formed by the microparticles injected into the main plasma with dispensers. We present here, as an example, the experiment performed with the main microparticle cloud composed of the monodisperse silica particles with the diameter of $1.55\ \mu\text{m}$. Neon was used as a buffer gas at pressures of 15 and 20 Pa. The observed projectiles were likely larger particles ($15\ \mu\text{m}$ in diameter) also present in the chamber [40].

We observed two events of the projectile motion through the dust cloud. Figure 8 shows one of them. The projectile moved with a supersonic velocity from the upper left to the lower right side of the dust cloud (Fig. 8(a)).

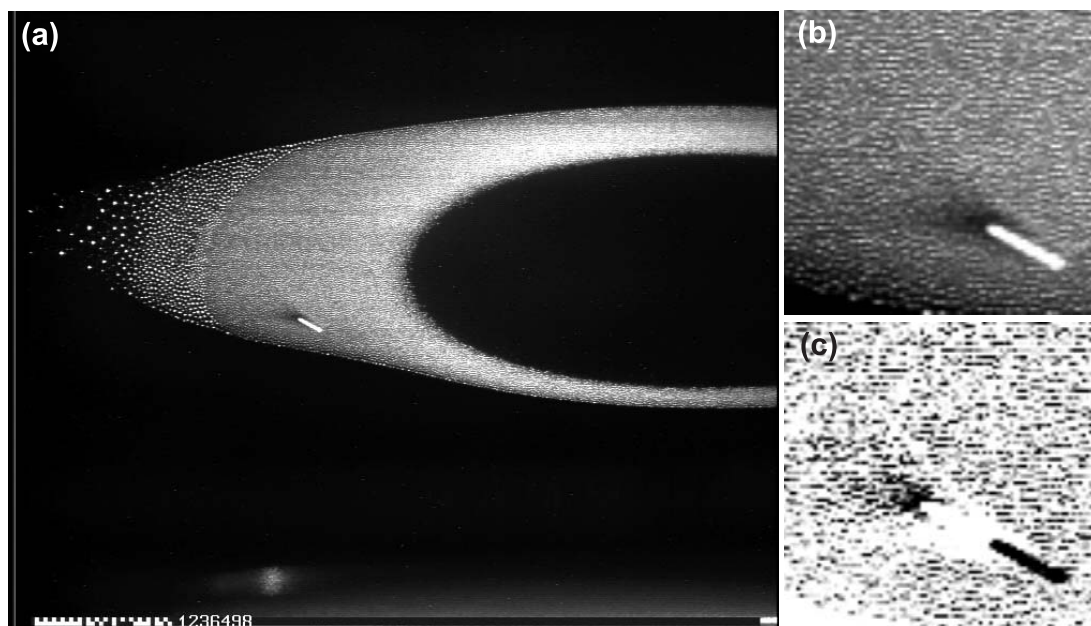


Fig. 8 a) Snapshot of the projectile moving through the cloud of dust particles with a supersonic speed. b) Enlarged fragment of the snapshot. c) The result of the Mach cone visualization. The neon gas pressure is 20 Pa.

The track of the moving projectile is surrounded by a dust-free region (cavity), which emerges as a result of a strong Coulomb repulsion between the negatively charged dust particles and the projectile Fig. 8(b). The cavity is elongated, the position of a projectile being eccentric. The perturbation has a typical form of the Mach cone, and represents a contact discontinuity [42].

The excitation of the Mach cone gives a possibility to measure the speed of sound, which is an important quantity characterizing the medium. The Mach angle, which is one-half of the opening angle of the cone excited by an object that moves through a fluid with a velocity v greater than the speed of sound c . The Mach angle θ is related to the Mach number M which gives the velocity with respect to the speed of sound by the Mach cone relation

$$\sin \theta = \frac{c}{v} = \frac{1}{M}.$$

In the experiment, the projectile velocity was determined by manual measurement of the positions of the projectile track centers in consequent frames (temporal resolution is 50 frames per second). The velocity proved to increase from 4.6 to 5.8 cm/s as the projectile crossed the dust cloud. The processing of the experimental results gives the speed of sound $c = 0.96 \pm 0.14$ cm/s for neon pressure of 15 Pa. The determined speed of sound turns out to be more than one order of magnitude lower than that predicted by the theory of the dust acoustic waves. Possible interpretation of this result has been discussed in ref. [41].

8 Conclusion

Experiments with three-dimensional complex plasmas performed in the PK-3 Plus laboratory on the International Space Station showed the variety and interdisciplinarity of the field. They allowed research at the most fundamental — the kinetic — level by observing individual particles in fluid-like and crystalline systems. Exemplarily the formation and melting of plasma crystals, laning in driven systems, electrorheological effects and, finally, the formation of Mach cones due to the penetration of projectiles through a dense complex plasma cloud were presented. Although the operation of the PK-3 Plus laboratory stopped in 2013, the promising research of large three-dimensional complex plasmas will be continued with the next microgravity laboratory, PK-4. This was launched in October 2014 and installed into the European Physiological Module in the Columbus Module. It is operational now and available for the next generation of experiments with complex plasmas under microgravity conditions onboard the ISS.

Acknowledgements The authors gratefully acknowledge the support from the Russian Science Foundation (Project No. 14-12-01235) and the support from DLR/BMWi (Grants No. 50WM0203 and 50WM1203).

References

- [1] V.E. Fortov and G.E. Morfill, *Complex and dusty plasmas, From Laboratory to Space*, CRC Press, 2010.
- [2] V.E. Fortov, A.V. Ivlev, S.A. Khrapak, A.G. Khrapak, and G.E. Morfill, *Phys. Rep.* **421**, 1 (2005).
- [3] A.P. Nefedov, G.E. Morfill, V.E. Fortov, H.M. Thomas, H. Rothermel, T. Hagl, A.V. Ivlev, M. Zuzic, B.A. Klumov, A.M. Lipaev, V.I. Molotkov, O.F. Petrov, Y.P. Gidzenko, S.K. Krikalev, W. Shepherd, A.I. Ivanov, M. Roth, H. Binnenbruck, J.A. Goree, and Y.P. Semenov, *New Journal of Physics* **5**, 33 (2003).
- [4] A.M. Lipaev, S.A. Khrapak, V.I. Molotkov, G.E. Morfill, V.E. Fortov, A.V. Ivlev, H.M. Thomas, A.G. Khrapak, V.N. Naumkin, A.I. Ivanov, S.E. Tretschew, and G.I. Padalka, *Phys. Rev. Lett.* **98**, 265006 (2007).
- [5] D. Samsonov, G.E. Morfill, H. Thomas, T. Hagl, H. Rothermel, V. Fortov, A. Lipaev, V. Molotkov, A. Nefedov, O. Petrov, A. Ivanov, and S. Krikalev, *Phys. Rev. E* **67**, 036404 (2003).
- [6] S. Khrapak, D. Samsonov, G.E. Morfill, H. Thomas, V. Yaroshenko, H. Rothermel, T. Hagl, V. Fortov, A. Nefedov, V. Molotkov, O. Petrov, A. Lipaev, A. Ivanov, and Y. Baturin, *Phys. Plasmas* **10**, 1 (2003).
- [7] S.A. Khrapak, A.V. Ivlev, G.E. Morfill, and H.M. Thomas, *Phys. Rev. E* **66**, 046414 (2002).
- [8] H.M. Thomas, G.E. Morfill, V.E. Fortov, A.V. Ivlev, V.I. Molotkov, A.M. Lipaev, T. Hagl, H. Rothermel, S.A. Khrapak, R.K. Suetterlin, M. Rubin-Zuzic, O.F. Petrov, V.I. Tokarev, and S.K. Krikalev, *New Journal of Physics* **10**, 033036 (2008).
- [9] H.M. Thomas and G.E. Morfill, *Nature* **379**, 806 (1996).
- [10] S.A. Khrapak, B.A. Klumov, P. Huber, V.I. Molotkov, A.M. Lipaev, V.N. Naumkin, H.M. Thomas, A.V. Ivlev, G.E. Morfill, O.F. Petrov, V.E. Fortov, Yu. Malentschenko, and S. Volkov, *Phys. Rev. Lett.* **106**, 205001 (2011).
- [11] H.J. Raveche, R.D. Mountain, and W. B. Streett, *J. Chem. Phys.* **61**, 1970 (1974).
- [12] S.A. Khrapak, B.A. Klumov, P. Huber, V.I. Molotkov, A. M. Lipaev, V.N. Naumkin, A.V. Ivlev, H.M. Thomas, M. Schwabe, G.E. Morfill, O.F. Petrov, V.E. Fortov, Yu. Malentschenko, and S. Volkov, *Phys. Rev. E* **85**, 066407 (2012).
- [13] P.J. Steinhardt, D.R. Nelson, and M. Ronchetti, *Phys. Rev. Lett.* **47**, 1297 (1981).
- [14] P.J. Steinhardt, D.R. Nelson, and M. Ronchetti, *Phys. Rev. B* **28**, 784 (1983).
- [15] S. Auer and D. Frenkel, *J. Chem. Phys.* **120**, 3015 (2004).
- [16] B.A. Klumov, P. Huber, S. Vladimirov, H. Thomas, A. Ivlev, G.E. Morfill, V. Fortov, A. Lipaev, and V. Molotkov, *Plasma Phys. Controlled Fusion* **51**, 124028 (2009).
- [17] D. Helbing, I.J. Farkas, and T. Vicsek, *Phys. Rev. Lett.* **84**, 1240 (2000).
- [18] M.E. Leunissen, C.G. Christova, A. Hynninen, C. Patrick Royall, A.I. Campbell, A. Imhof, M. Dijkstra, R. van Roij and A. van Blaaderen, *Nature* **437**, 235 (2005).
- [19] J. Dzubiella, G.P. Hoffmann, and H. Löwen, *Phys. Rev. E* **65**, 021402 (2002).
- [20] B. Schmittmann and R.K.P. Zia, *Phys. Rep.* **301**, 45 (1998).
- [21] R.R. Netz, *Europhys. Lett.* **63**, 616 (2003).
- [22] K.R. Sutterlin, A. Wysocki, A.V. Ivlev, C. Rath, H.M. Thomas, M. Rubin-Zuzic, W.J. Goedheer, V.E. Fortov, A.M. Lipaev, V.I. Molotkov, O.F. Petrov, G.E. Morfill, and H. Lowen, *Phys. Rev. Lett.* **102**, 085003 (2009).
- [23] V.I. Molotkov, A.M. Lipaev, V.N. Naumkin, H.M. Thomas, M. Schwabe, A.V. Ivlev, S.A. Khrapak, V.E. Fortov, and G.E. Morfill, *Dusty/complex plasmas, basic and interdisciplinary research, sixth international conference on the physics of dusty plasmas*, *AIP Proc.* **1397**, 377 (2011).
- [24] A.V. Ivlev, G.E. Morfill, H.M. Thomas, C. Rath, G. Joyce, P. Huber, R. Kompaneets, V.E. Fortov, A.M. Lipaev, V.I. Molotkov, T. Reiter, M. Turin, and P. Vinogradov, *Phys. Rev. Lett.* **100**, 095003 (2008).

- [25] O. Havnes, T. Aslaksen, T.W. Hartquist, F. Li, F. Melandsø, G.E. Morfill, and T. Nitter, *J. Geophys. Res.* **100**, 1731 (1995).
- [26] O. Havnes, F. Li, F. Melandsø, T. Aslaksen, T.W. Hartquist, G.E. Morfill, T. Nitter, and V. Tsytovich, *J. Vac. Sci. Technol. A* **14**, 525 (1996).
- [27] D. Samsonov, J. Goree, Z.W. Ma, A. Bhattacharjee, H.M. Thomas, and G.E. Morfill, *Phys. Rev. Lett.* **83**, 3649 (1999).
- [28] D. Samsonov, J. Goree, H.M. Thomas, and G.E. Morfill, *Phys. Rev. E* **61**, 5557 (2000).
- [29] A. Melzer, S. Nunomura, D. Samsonov, Z.W. Ma, and J. Goree, *Phys. Rev. E* **62**, 4162 (2000).
- [30] V. Nosenko, J. Goree, Z.W. Ma, and A. Piel, *Phys. Rev. Lett.* **88**, 135001 (2002).
- [31] V. Nosenko, J. Goree, Z.W. Ma, D. Dubin, and A. Piel, *Phys. Rev. E* **68**, 056409 (2003).
- [32] D. Dubin, *Phys. Plasmas* **7**, 3895 (2000).
- [33] S. Zhdanov, S. Nunomura, D. Samsonov, and G.E. Morfill, *Phys. Rev. E* **68**, 035401 (2003).
- [34] K. Jiang, L.J. Hou, Y.N. Wang, and Z.L. Mišković, *Phys. Rev. E* **73**, 016404 (2006).
- [35] L.J. Hou, Y.N. Wang, and Z.L. Mišković, *Phys. Rev. E* **70**, 056406 (2004).
- [36] O. Havnes, F. Li, T.W. Hartquist, T. Aslaksen, and A. Brattli, *Planet. Space Sci.* **49**, 223 (2001).
- [37] A.A. Mamun, P.K. Shukla, and G.E. Morfill, *Phys. Rev. Lett.* **92**, 095005 (2004).
- [38] S. Zhdanov, G.E. Morfill, D. Samsonov, M. Zuzic, and O. Havnes, *Phys. Rev. E* **69**, 026407 (2004).
- [39] K. Jiang, V. Nosenko, Y.F. Li, M. Schwabe, U. Konopka, A.V. Ivlev, V.E. Fortov, V.I. Molotkov, A.M. Lipaev, O.F. Petrov, M.V. Turin, H.M. Thomas, and G.E. Morfill, *Europhys. Lett.* **85**, 4500 (2009).
- [40] M. Schwabe, K. Jiang, S. Zhdanov, T. Hagl, P. Huber, A.V. Ivlev, A.M. Lipaev, V.I. Molotkov, V.N. Naumkin, K.R. Sütterlin, H.M. Thomas, V.E. Fortov, G.E. Morfill, A. Skvortsov, and S. Volkov, *Europhys. Lett.* **96**, 55001 (2011).
- [41] D.I. Zhukhovitskii, V.E. Fortov, V.I. Molotkov, A.M. Lipaev, V.N. Naumkin, H.M. Thomas, A.V. Ivlev, M. Schwabe, and G.E. Morfill, *Phys. Plasmas* **22**, 023701 (2015).
- [42] L.D. Landau and E.M. Lifshitz, *Fluid Mechanics*, Pergamon Press, New York, 1959.